
NEAT: Neighborhood-Guided, Efficient, Autoregressive Set Transformer for 3D Molecular Generation

Daniel Rose^{* 1 2 3} Roxane Axel Jacob^{* 1 2 3} Johannes Kirchmair^{1 2} Thierry Langer^{1 2}

Abstract

Autoregressive models are a promising alternative to diffusion-based models for 3D molecular structure generation. However, a key limitation is the assumption of a token order: while text has a natural sequential order, the next token prediction given a molecular graph prefix should be invariant to atom permutations. Previous works sidestepped this mismatch by using canonical orders or focus atoms. We argue that this is unnecessary. We introduce NEAT, a Neighborhood-guided, Efficient, Autoregressive, Set Transformer that treats molecular graphs as sets of atoms and learns the order-agnostic distribution over admissible tokens at the graph boundary with an autoregressive flow model. NEAT approaches state-of-the-art performance in 3D molecular generation with high computational efficiency and atom-level permutation invariance, establishing a practical foundation for scalable molecular design.

1. Introduction

Computational workflows for discovering bioactive molecules often rely on either virtual screening of compound libraries or fragment spaces (Warr et al., 2022), or direct *de novo* generation of compounds with desired properties (Peng et al., 2023). Although the expansion of chemical spaces increases the odds that the right design will be found, their growing sizes make screening increasingly computationally expensive (Bellmann et al., 2022). Moreover, despite their ultra-large sizes, chemical spaces still encompass

only a small fraction of the vast molecular design space.

Conditional molecular generation offers a promising alternative to virtual screening by enabling the computationally cheaper generation of new molecules based on user-defined constraints. It can be approached through the generation of (1D) SMILES strings (Gómez-Bombarelli et al., 2018; Kusner et al., 2017), (2D) molecular graphs (Simonovsky & Komodakis, 2018; Cao & Kipf, 2022), (3D) atomic point clouds (Gebauer et al., 2019; Satorras et al., 2021; Hoogeboom et al., 2022; Luo & Ji, 2022; Xu et al., 2023; Daigavane et al., 2024; Zhang et al., 2025; Cheng et al., 2025), or a combination thereof (Hua et al., 2023; Peng et al., 2023; Vignac et al., 2023). Because molecules are inherently three-dimensional, with many properties determined by their conformations, 3D generation is the self-evident choice. In this work, we focus on unconditional 3D generation, which is a necessary prerequisite to condition the generation process towards compounds with specific biological functions later on (Peng et al., 2022; Schneuing et al., 2024).

State-of-the-art 3D molecular generation models rely on diffusion and flow matching techniques (Hoogeboom et al., 2022; Xu et al., 2023; Song et al., 2024; Zhang et al., 2025; Feng et al., 2025; Song et al., 2023; Dunn & Koes, 2025). A key limitation of these methods is the need to compute the joint atom distribution at each diffusion step through computationally intensive, quadratically scaling message-passing updates in the encoder model to capture atom interdependencies. Additionally, diffusion and flow matching molecular generators require the number of atoms to be predefined. While the use of dummy atoms offers a partial workaround (Adams et al., 2025; Dunn & Koes, 2025), these approaches remain constrained by the upper bound on the number of nodes sampled from the noise distribution.

Autoregressive models offer a flexible and efficient alternative. They support variable atom counts and require only one encoder call per generated token (Li et al., 2024). For 3D autoregressive molecular generation, there exists 3 lines of work: (1) using graph neural networks (GNNs) in combination with focus atoms (Gebauer et al., 2019; Luo & Ji, 2022; Daigavane et al., 2024); (2) using standard large language models (LLMs) for generating XYZ, CIF or PDB files (Flam-Shepherd & Aspuru-Guzik, 2023) or SE(3)-invariant

¹Department of Pharmaceutical Sciences, Division of Pharmaceutical Chemistry, Faculty of Life Sciences, University of Vienna, Josef-Holaubek-Platz 2, 1090 Vienna, Austria ²Christian Doppler Laboratory for Molecular Informatics in the Biosciences, Department of Pharmaceutical Sciences, University of Vienna, Josef-Holaubek-Platz 2, 1090 Vienna, Austria ³Vienna Doctoral School of Pharmaceutical, Nutritional and Sport Sciences, University of Vienna, Josef-Holaubek-Platz 2, 1090 Vienna, Austria. Correspondence to: <first.middle.last@univie.ac.at>.

1D tokens (Li et al., 2025b; Fu et al., 2025; Lu et al., 2025); (3) combining a causal transformer with a diffusion loss to generate continuous tokens (atomic coordinates) (Cheng et al., 2025; Li et al., 2025a). Although current GNN-based methods ensure permutation invariance with respect to atom ordering, they generate molecules with low chemical validity. Conversely, sequence-based methods perform well in terms of validity but are not permutation-invariant with respect to atom ordering.

In this work, we present the first autoregressive transformer model for 3D molecular generation that respects the atom permutation-invariance of molecular graphs. Working without canonical atom orderings introduces two challenges. First, it precludes the use of sequence embeddings, which are an essential component of standard autoregressive models. To address this, we model atomic interdependencies within the growing molecular graph using a set transformer (Lee et al., 2019). Second, it changes the autoregressive training set-up from supervision with a single token per step to supervision with a set of valid tokens: without a canonical atom order, all atoms in the 1-hop neighborhood of the current graph are valid continuations.

Our solution to this challenge is conceptually simple and effective. Given a partial molecular graph, the model is trained to produce a token distribution that matches the boundary nodes of the subgraph (i.e., the 1-hop neighbors of existing nodes). We refer to this training signal as neighborhood guidance. This yields a probabilistic next-token distribution without relying on ad hoc canonicalization schemes. We combine this with a flow-matching loss to model continuous atomic coordinates. Our model, NEAT (Neighborhood-guided, Efficient Autoregressive set Transformer), achieves competitive performance relative to state-of-the-art 3D generative models while maintaining permutation invariance to atom ordering.

We expect these contributions to advance the development of autoregressive methods for *de novo* 3D molecular design and to provide a solid foundations for conditional molecular generation.

2. Related works

Autoregressive models generate sequences of tokens by conditioning each token on its predecessors. Formally, given a token sequence $x = (x_1, \dots, x_N)$, the joint distribution $p(x)$ is factorized as:

$$p(x) = \prod_{n=1}^{N-1} p(x_{n+1} | x_{:n}), \quad (1)$$

where $x_{:n} = (x_1, \dots, x_n)$ represents the tokens up to step n . Sampling is performed by initializing with x_1 and sequentially generating tokens until x_N . This is straightforward

for sequentially ordered data such as text or images. In the graph domain, the generation order is less obvious, and has been an active focus of research. One way to model graphs as sequences is through canonicalization. However, predefined canonical orderings impose limitations, as the optimal generation order is often context-dependent. To alleviate strict assumptions, You et al. (2018) proposed a breadth-first search (BFS) node ordering for autoregressive graph generation, while Wang et al. (2025b) introduced order policies to dynamically assign generation orders based on the current state. Although these approaches reduce reliance on fixed orderings, they do not fully eliminate order dependence. 3D molecules are geometric graphs whose structure is determined by connectivity and geometry. The generation of valid positions poses additional constraints on the graph generation process and recent work on this specific task will be discussed in the following.

GNN models with focus atoms G-SchNet (Gebauer et al., 2019) is an $E(3)$ -invariant GNN model that introduces the concept of focus atoms for generation order. In each generation step, the model selects a focus atom as the center of a 3D grid, chooses the next atom type, and infers its position probability from radial distances to previously placed atoms. G-SphereNet (Luo & Ji, 2022) adopts this approach but places atoms relative to the focus atom by generating distances, angles, and torsions with a normalizing flow. The $E(3)$ -equivariant Symphony model (Daigavane et al., 2024) parameterizes the 3D probability around the focus atom using $E(3)$ -equivariant features from spherical harmonic projections rather than rotationally invariant features. While these models respect the permutation-invariance of atoms, they produce molecules with comparably low chemical validity.

Transformer models with tokenization Transformers can be used for 3D molecule generation when combined with a suitable text format. Flam-Shepherd & Aspuru-Guzik (2023) trained an LLM for 3D molecular generation directly on XYZ, CIF, or PDB files. An active line of research are tokenization schemata to allow LLMs more fine-grained control in the generation process. Geo2Seq (Li et al., 2025b) converts molecular geometries into $SE(3)$ -invariant 1D discrete sequences for unconditional modeling, while Frag2Seq (Fu et al., 2025) introduces a related technique for structure-based modeling. Lu et al. (2025) employs a voxel-based discretization scheme with an octree-based compression technique, yielding sparse sequences.

Transformer models without vector quantization One of the challenges in generating 3D molecular structures with transformers is to generate continuous-valued tokens like 3D atomic coordinates without discrete tokenization strategies. While standard transformer architectures were

initially developed for categorical data, they can be adapted for the generation of continuous values. Li et al. (2024) directly models the next-token distribution $p(x_{n+1} | x_{:n})$ using a diffusion-based approach, factorized as:

$$p(x_{n+1} | x_{:n}) = p(x_{n+1} | \mathbf{z}_n) \cdot p(\mathbf{z}_n | x_{:n}), \quad (2)$$

where $\mathbf{z}_n \in \mathbb{R}^k$ represents an abstract latent variable for the next token. This factorization enables to use a transformer to model $p(\mathbf{z}_n | x_{:n})$ to capture interdependencies among tokens, followed by a lightweight diffusion-based MLP to map \mathbf{z}_n to the continuous token space. Their approach demonstrated high-quality autoregressive image generation with improved inference speed.

Recent work successfully applied the diffusion loss to the generation of atomic positions, enabling 3D molecular generation without tokenization. Cheng et al. (2025) employed a causal transformer with sequential embeddings derived from the atom order in XYZ coordinate files to predict discrete atom types, and a diffusion model, conditioned on these predictions, to predict the corresponding continuous 3D atom positions. However, the study also shows that reliance on a causal transformer introduces limitations. The use of sequence information based on atom order in XYZ files makes the model susceptible to overfitting and degrades performance when the atom order is perturbed. (Li et al., 2025a) adopt a comparable framework, adding inertial-frame alignment for coordinates and canonical atom ordering, but their method only relocates the problem of token-order sensitivity rather than eliminating it.

We propose that a set transformer (Lee et al., 2019) with bidirectional attention is better suited for autoregressive 3D molecular generation, as it inherently respects the permutation invariance of atom sets by disregarding generation order at state n . This raises the challenge of compensating for the absence of sequential order information, which is the key focus of our work.

3. Methods

Overview Our architecture consists of three main components: (1) a data-augmentation module that provides neighborhood-guidance during training, (2) a set transformer trunk that produces permutation-invariant encodings of atom sets, and (3) a flow-matching head that generates continuous atomic coordinates. During training, we split molecules into a source set, representing the state of the molecular graph at step n , and a target set, representing the set of possible token continuations at step $n + 1$. The source set is processed by the set transformer to obtain a learned representation of the current state. This source set representation is then passed through a simple linear layer followed by a softmax to yield a categorical distribution over the next atoms’ types. The continuous next atoms’ positions

are modeled by the flow matching head, conditioned on the source set representation and the next atom type. During training, we use teacher forcing to decouple the prediction of atom types from the prediction of atom positions. Because the expensive source set representation is computed only once per generated token, our model is computationally more efficient than non-autoregressive frameworks that rely entirely on diffusion or flow-matching. Training and inference procedures are summarized in Figures 1 and 2, respectively.

Molecular representation Molecules are represented as undirected graphs $G = (V, E, \mathbf{a}, \mathbf{X})$, where $V = [N]$ is the set of node indices, $E \subseteq \{\{i, j\} : 1 \leq i < j \leq N\}$ is the set of undirected edges, atom types $\mathbf{a} \in \mathcal{A}^N$ are elements of the vocabulary \mathcal{A} and positions $\mathbf{X} \in \mathbb{R}^{N \times 3}$ are the Cartesian coordinates after zero-centering the molecular graph. The vocabulary \mathcal{A} is the set of possible element types and a special stop token, which stops the autoregressive generation process. A subgraph $G' = (V', E')$ of G , denoted by $G' \subseteq G$, is defined as a subset of the nodes $V' \subseteq V$ and edges $E' \subseteq E$. Furthermore, $G' = G[V']$ is a node-induced subgraph of G , if $E' = (V' \times V') \cap E$. A connected graph contains at least one path between any pair of vertices, and a path is defined as a sequence of vertices (v_0, \dots, v_n) with $(v_i, v_{i+1}) \in E$ for $0 \leq i < n$. The neighborhood of a node index i is the set of all adjacent node indices $\mathcal{N}(i) = \{j \in V : (i, j) \in E\}$. Given a node-induced subgraph $G[V']$, we further define the set of boundary nodes $\partial V' = (\bigcup_{i \in V'} \mathcal{N}(i)) \setminus V'$. Finally, given a node subset V' , we denote the corresponding subset of atom types as $\mathbf{a}[V']$ and the subset of atom positions as $\mathbf{X}[V']$.

Autoregressive 3D molecular graph generation In a build-up phase, the model iteratively predicts atom type a_{n+1} and position \mathbf{x}_{n+1} , given the current set of atoms and positions at step n . We will use the following compact notation $\mathbf{a}_{1:n} = (a_1, \dots, a_n)$ to refer to the generated atom types and positions $\mathbf{X}_{1:n} = (\mathbf{x}_1, \dots, \mathbf{x}_n)$ at step n . The autoregressive build-up stops when the model predicts a stop token. Edges are then inferred from the N generated atoms via a predefined set of rules like $E = \mathcal{R}(\mathbf{a}, \mathbf{X})$, which completes inference of the molecular graph G . While edges are inferred from atom types and positions after the build-up phase, the edge information can still be used for teacher guidance in the training phase. In the following, we describe how we use this information for model training.

Neighborhood guidance We propose a sampling strategy that mimics molecular growth during the autoregressive build-up phase. Given a molecule G in the training set, we sample a node-induced, connected subgraph $G[V_S]$ of the molecular graph G . We call V_S the *source set*. $G[V_S]$ simulates a valid molecular fragment with atom

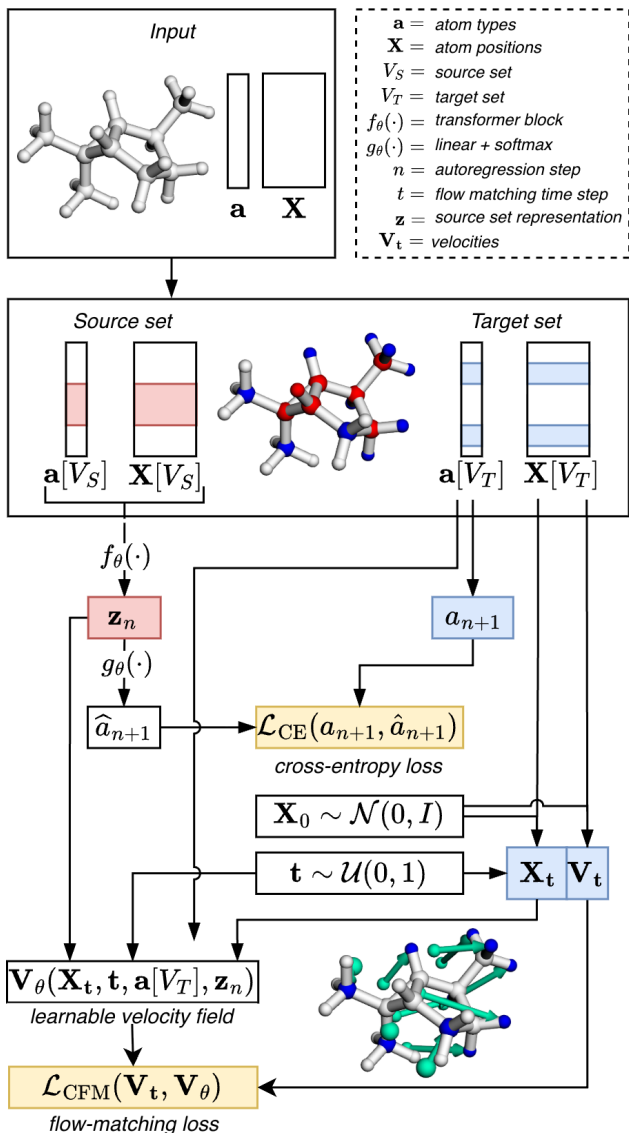


Figure 1. Overview of the proposed training workflow. The model takes molecular graphs as input, where nodes encode atom types and positions, and edges represent chemical bonds. For each training example, we randomly sample a connected subgraph. The selected nodes form the source set, and their neighboring boundary nodes define the target set. The source set is encoded using a set transformer, and its representation is used to predict the distribution over the next atom type. For each target-set node, we sample a position from a normal distribution and construct linear interpolation paths between the sampled and true positions. These interpolation paths provide supervision for learning the vector field via flow matching.

types $\mathbf{a}[V_S] = \mathbf{a}_{1:n}$ and positions $\mathbf{X}[V_S] = \mathbf{x}_{1:n}$ in the autoregressive build-up at step $n = |V_S|$. The *target set* V_T is the set of valid token continuations at step $n + 1$. It is the set of boundary nodes ∂V_S , given V_S , and induces atom types $\mathbf{a}[V_T]$ and positions $\mathbf{X}[V_T]$ for model supervision.

Algorithm 1 Source-Target Split Augmentation

Input: Graph $G = (V, E)$, β, γ
 $v_0 = \text{RandomNode}(V)$
 $V_S = \{v_0\}$
 $m = \beta \cdot \text{RandomUniform}(0, \epsilon(v_0))$
for $i = 0$ **to** $m - 1$ **do**
 $\partial V_S \leftarrow (\bigcup_{i \in V_S} \mathcal{N}(i)) \setminus V_S$
 $\partial V_S \leftarrow \{v \in \partial V' \mid \text{RandomUniform}(0, 1) > \gamma\}$
 $V_S \leftarrow V_S \cup \partial V_S$
end for
 $V_T \leftarrow (\bigcup_{i \in V_S} \mathcal{N}(i)) \setminus V_S$
Return: V_S, V_T

The sampling of connected subgraphs is performed dynamically during training. First, we precompute the eccentricity $\epsilon(v)$ for each node $v \in V$ in the molecular graph. During runtime, a random seed node v_0 is selected from each molecule in the batch. Starting from this seed atom, we perform m rounds of 1-hop neighborhood aggregation, where m is a random number between 0 and $\epsilon(v_0)$. This process generates connected subgraphs of varying sizes, ranging from a single node to the entire molecular graph.

To avoid biasing the sampling process toward globular subgraphs, we introduce stochasticity by randomly dropping a subset of the boundary nodes before aggregation, controlled by a dropout factor γ . To counteract the resulting bias toward smaller subgraphs, we introduce a scaling parameter β , which adjusts the number of growth iterations per graph. By balancing these two parameters, our sampling strategy generates connected subgraphs of diverse sizes and shapes, effectively simulating molecular growth during autoregressive generation. The pseudo-code for our sampling strategy is provided in Algorithm 1. In practice, this sampling strategy is efficiently implemented using batched operations and introduces only minimal overhead to the training process, which is dominated by the forward passes through the transformer.

Transformer trunk The computation of the source set representation $f_\theta : (\mathbf{a}_{1:n}, \mathbf{X}_{1:n}) \rightarrow \mathbf{z}_n$ at step n is straightforward. Atom types $\mathbf{a}_{1:n}$ are encoded using a linear embedding layer, while their positions $\mathbf{X}_{1:n}$ are encoded with Fourier features (Tancik et al., 2020). The summation of these encodings produces the initial node representations. For the transformer backbone f_θ , we adopt the NanoGPT implementation (Karpathy, 2025) of GPT-2 (Radford et al., 2019), removing positional sequence embeddings and replacing causal attention with bidirectional attention. After the transformer updates, the node representations are aggregated by additive pooling (Zaheer et al., 2017) to form a set-level representation \mathbf{z}_n , which characterizes the current source set at step n .

Next token prediction The set-level representation \mathbf{z}_n is used to model the distribution of possible next tokens, represented as the joint distribution $p(a_{n+1}, \mathbf{x}_{n+1} \mid \mathbf{z}_n)$, which is factorized as follows:

$$p(a_{n+1}, \mathbf{x}_{n+1} \mid \mathbf{z}_n) = p(a_{n+1} \mid \mathbf{z}_n) \cdot p(\mathbf{x}_{n+1} \mid a_{n+1}, \mathbf{z}_n), \quad (3)$$

where $p(a_{n+1} \mid \mathbf{z}_n)$ represents the distribution over the next atom types, and $p(\mathbf{x}_{n+1} \mid a_{n+1}, \mathbf{z}_n)$ models the distribution over the next atom positions given the next atom type. The next atom type probability $p(a_{n+1} \mid \mathbf{z}_n)$ is modeled as a categorical distribution over the vocabulary of atom types and is approximated with a linear layer followed by a softmax operation $g_\theta : \mathbf{z}_n \rightarrow \hat{a}_{n+1}$. For model supervision, we compute the mean over the one-hot-encoded atom types in the target set $\hat{a}_{n+1} = \text{mean}(\text{onehot}(\mathbf{a}[V_T]))$ and apply a cross-entropy loss.

The next atom position is modeled as a conditional distribution given the next atom type. We model this distribution via flow matching (Lipman et al., 2023; Albergo & Vanden-Eijnden, 2023) (see Appendix Section A.1 for a more detailed description of the formalism). During training, we employ teacher forcing to decouple the atom type prediction from the task of positional recovery. For the set of possible next positions $\mathbf{X}_1 = \mathbf{X}[V_T]$ corresponding to the target set V_T , we sample a set of random initial positions $\mathbf{X}_0 \sim p_0$, where $p_0 = \mathcal{N}(0, \sigma^2 I)$. Following the flow matching convention, we construct interpolation paths between the positions at the random position at $t = 0$ and the true position at $t = 1$:

$$\mathbf{X}_t = (1 - t) \cdot \mathbf{X}_0 + t \cdot \mathbf{X}_1 \quad (4)$$

with random time steps $t \in \mathcal{U}(0, 1)^{|V_T|}$, yielding a set of interpolated positions \mathbf{X}_t with velocities $\mathbf{V}_t = \mathbf{X}_1 - \mathbf{X}_0$. We then train the conditional vector field \mathbf{V}_θ through regression against the set of CFM path velocities:

$$\mathcal{L}_{\text{CFM}} = \frac{1}{|V_T|} \|\mathbf{V}_\theta(\mathbf{X}_t, t, \mathbf{a}[V_T], \mathbf{z}_n) - \mathbf{V}_t\|_2^2 \quad (5)$$

Note that this equation does not require sequential information as input. The vector field \mathbf{V}_θ is parametrized with the adaptive layer MLP from (Li et al., 2024).

Distributional coupling and optimal transport In order to reduce the transport cost between the source distribution p_0 and the target distribution p_1 , we employ a simple coupling scheme. Given the positions \mathbf{X}_1 and \mathbf{X}_0 , we solve the linear assignment problem on the distance matrix $\mathbf{X}_1^T \mathbf{X}_0$ and permute the positions in \mathbf{X}_0 accordingly. This procedure avoids crossing paths, resulting in improved performance.

Inference The molecular generation process begins by randomly sampling an initial atom type a_1 from the atom

type vocabulary \mathcal{A} and drawing its initial position $\mathbf{x}_1 \in \mathbb{R}^3$ from a normal distribution $\mathcal{N}(0, \sigma^2 I)$. At each subsequent autoregressive step, the current atom set $(\mathbf{a}_{1:n}, \mathbf{X}_{1:n})$ is passed through the transformer, producing the set-level representation \mathbf{z}_n . The next atom type a_{n+1} is predicted from \mathbf{z}_n using a linear layer followed by the softmax function. A random initial position \mathbf{x}_{n+1} is then sampled from $\mathcal{N}(0, \sigma^2 I)$, and the flow ODE is integrated from $t = 0$ to $t = 1$ using Euler integration to compute the next atom position. This iterative process continues until a stop token is predicted, signaling the end of the molecular generation. The workflow is illustrated in Figure 2. Molecular generation is efficiently implemented using batched operations, enabling parallel generation and high computational speed. Although bidirectional attention precludes the use of query-value caching, our generation process remains fast in practice.

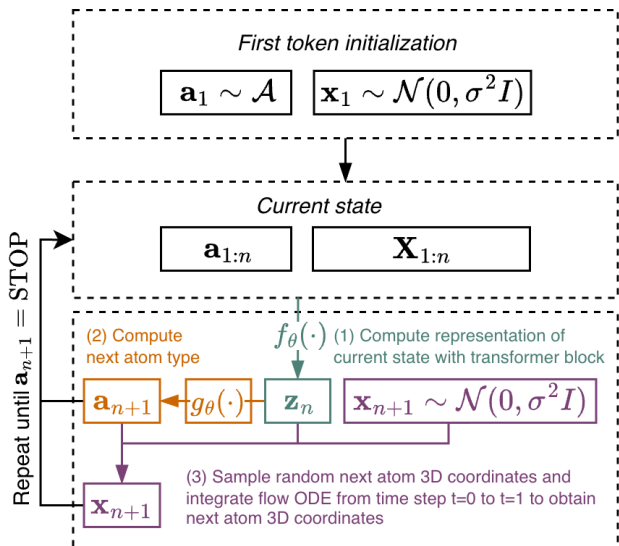


Figure 2. Overview of the proposed model inference workflow.

4. Experiments

Data We trained NEAT on the QM9 dataset, a collection of small organic molecules composed of hydrogen (H), carbon (C), nitrogen (N), oxygen (O), and fluorine (F) atoms. The dataset includes molecules with up to 9 heavy atoms (C, N, O, F) and a total of 29 atoms when hydrogen is included (Ramakrishnan et al., 2014). Following Hoogeboom et al. (2022), we split the dataset into 100,000 molecules for training, 17,748 for validation, and 13,083 for testing.

Evaluation metrics To evaluate the quality of generated molecules, we adhere to standard practices (Hoogeboom et al., 2022; Zhang et al., 2025; Cheng et al., 2025) and report atomic and molecular stability, molecular validity, and molecular uniqueness. An atom is considered stable if its

Table 1. Performance comparison of NEAT with autoregressive models trained on the QM9 dataset. All values are given in percent. The **best** and **second-best** performing models are highlighted. Models evaluated using our pipeline are marked with a star (*). Metrics are reported as the mean and 95% confidence interval over three runs, each generating 10,000 molecular designs. Results in the top row are computed on the QM9 test set of 13,083 molecules.

metrics	atom stab.	mol. stab.	lookup valid	lookup unique	xyz2mol valid	xyz2mol unique
QM9	99.4	95.3	97.7	97.7	100	100
G-SchNet	95.7	68.1	85.5	80.3	75.0	72.5
Symphony	90.8	43.9	68.1	66.5	83.5	81.8
Geo2Seq	98.9	93.2	97.1	81.7	n.a.	n.a.
QUETZAL*	<u>98.3</u>	<u>87.5</u>	<u>94.6</u>	90.1	99.3	<u>94.4</u>
	± 0.1	± 0.1	± 0.1	± 0.2	± 0.1	± 0.1
NEAT* (ours)	98.2	84.7	93.4	<u>88.6</u>	<u>98.5</u>	94.8
	± 0.1	± 0.4	± 0.3	± 0.4	± 0.1	± 0.1

valence is valid (i.e., it satisfies the octet or duet rule given its formal charge and environment). A molecule is defined as stable if all of its atoms are stable. Molecular validity is assessed using two approaches: (1) the widespread EDM pipeline (Hoogeboom et al., 2022) based on bond lookup tables; (2) the pipeline introduced by Daigavane et al. (2024) and adopted by Cheng et al. (2025), where a molecule is deemed valid if bonds can be assigned using RDKit’s MolFromXYZBlock function and rdDetermineBonds module (version 2023.3.3), which uses the xyz2mol package based on the work of Kim & Kim (2015). Molecular uniqueness is the percentage of distinct canonical SMILES strings derived from valid molecules and can therefore be thought of as the percentage of valid and unique designs. For all metrics, we generate 10,000 samples and report the mean value and 95% confidence interval across three runs.

Baselines We compare NEAT to three autoregressive 3D molecular generation models (G-SchNet (Gebauer et al., 2019), Symphony (Daigavane et al., 2024), QUETZAL (Cheng et al., 2025)) and one model-agnostic method to convert 3D molecular structures into SE(3)-invariant 1D discrete sequences that is used in combination with language models to generate 3D molecules (Geo2Seq (Li et al., 2025b)). Results can be found in Table 1. Additional results comparing NEAT to diffusion models can be found in the Appendix. To ensure fair comparisons, we utilized the source code and pre-trained models of the baseline methods, where available, to generate molecules and evaluate their performance using our pipeline. Random examples of generated molecules are provided in Figure 3.

Model performance Model rankings depend on how bonds are inferred from generated point clouds. We report metrics using the lookup method proposed by EDM because it is widely adopted and thus facilitates fair comparisons. A

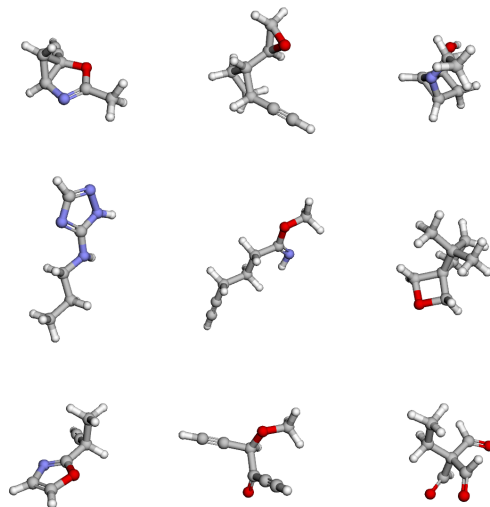


Figure 3. Randomly selected examples of generated molecules (white: hydrogen, gray: carbon, purple: nitrogen, red: oxygen).

notable limitation is the absence of aromatic bond handling and high sensitivity to bond lengths (Daigavane et al., 2024), which yields systematically lower scores for valid aromatic structures and thus reduces the informative value of these metrics. We further report molecular validity and uniqueness using the xyz2mol method. The conceptually related G-SchNet and Symphony models underperform in terms of all metrics. Geo2Seq obtains the highest scores for atom stability, molecular stability, and (lookup) molecular validity, followed by QUETZAL. However, Geo2Seq performs poorly on molecular uniqueness, which is the metric we consider most critical for downstream applications such as drug discovery. Valid designs are of limited value if they do not span a broad chemical space, and low molecular uniqueness might indicate overfitting to the training data. NEAT outperforms all models in terms of xyz2mol uniqueness, and is a close second to QUETZAL on lookup uniqueness and xyz2mol validity. Additionally, unlike QUETZAL and Geo2Seq, NEAT enforces atom-level permutation invariance and avoids sequential positional encodings, which is essential for prefix completion in molecular design. NEAT’s runtime for generating 10,000 molecules is 105 seconds, slightly faster than QUETZAL’s 134 seconds, indicating that bidirectional attention introduces no practical overhead relative to causal attention. Runtimes are averaged over three runs on a system with an AMD Ryzen 9 7950X 16-core CPU and an NVIDIA GeForce RTX 4090 GPU.

Limitations Our model inherits standard limitations of autoregressive decoders. Error propagation might degrade sampling for larger molecules, which could be mitigated by a self-correction mechanism in future work. Our model

produces variable-sized molecules, but does not extrapolate beyond the maximum atom count seen during training. For large molecules, pooling node embeddings may cause oversquashing and lose key information. Because bonds are not predicted explicitly, bond assignments still rely on predefined rules. Finally, despite random rotations during training, the lack of $SE(3)$ equivariance can yield orientation-dependent predictions.

5. Conclusion

We introduce a new method for training an autoregressive transformer with bidirectional attention for 3D molecular generation using neighborhood guidance. Instead of sequential positional encodings, we rely on a subgraph sampling schema for model supervision. Treating the input as a permutation-invariant set removes the need for sequence canonicalization and makes the model well-suited for prefix completion. On QM9, our approach achieves competitive performance, while offering permutation-invariance with respect to atoms and fast sampling. We believe this provides a strong foundation for future work in conditional modeling and autoregressive models.

Software and Data

Code and model weights will be made publicly available upon acceptance.

Impact Statement

This paper presents work whose goal is to advance the field of Machine Learning. There are many potential societal consequences of our work, none which we feel must be specifically highlighted here.

Acknowledgements

The financial support received for the Christian Doppler Laboratory for Molecular Informatics in the Biosciences by the Austrian Federal Ministry of Labour and Economy, the National Foundation for Research, Technology and Development, the Christian Doppler Research Association, Boehringer-Ingelheim RCV GmbH & Co KG and BASF SE is gratefully acknowledged.

Author contributions

Conceptualization: DR, RAJ. Methodology: DR, RAJ. Investigation: DR, RAJ. Data curation & analysis: DR, RAJ. Code implementation & model training: DR, RAJ. Writing (original draft): DR, RAJ. Writing (review and editing): DR, RAJ, JK. Funding acquisition: JK, TL. Resources: JK, TL. Supervision: JK, TL. All authors approved the final version

of the manuscript.

References

- Adams, K., Abeywardane, K., Fromer, J., and Coley, C. W. ShEPHERD: Diffusing shape, electrostatics, and pharmacophores for bioisosteric drug design. In *Proceedings of the 13th International Conference on Learning Representations*. Curran Associates, Inc., 2025.
- Albergo, M. S. and Vanden-Eijnden, E. Building normalizing flows with stochastic interpolants. In *Proceedings of the 11th International Conference on Learning Representations*. Curran Associates, Inc., 2023.
- Bellmann, L., Penner, P., Gastreich, M., and Rarey, M. Comparison of combinatorial fragment spaces and its application to ultralarge make-on-demand compound catalogs. *J. Chem. Inf. Model.*, 62:553–566, 2022. doi: 10.1021/acs.jcim.1c01378.
- Cao, N. D. and Kipf, T. MolGAN: An implicit generative model for small molecular graphs, 2022. URL <https://arxiv.org/abs/1805.11973>.
- Cheng, A. H., Sun, C., and Aspuru-Guzik, A. Scalable autoregressive 3D molecule generation, 2025. URL <https://arxiv.org/abs/2505.13791>.
- Daigavane, A., Kim, S. E., Geiger, M., and Smidt, T. Symphony: Symmetry-equivariant point-centered spherical harmonics for 3D molecule generation. In *Proceedings of the 12th International Conference on Learning Representations*. Curran Associates, Inc., 2024.
- Dunn, I. and Koes, D. R. FlowMol3: Flow matching for 3D de novo small-molecule generation, 2025. URL <https://arxiv.org/abs/2508.12629>.
- Falcon, W. and the PyTorch Lightning team. Pytorch lightning, 2025. URL <https://github.com/Lightning-AI/lightning>.
- Feng, S., Ni, Y., yan, L., Ma, Z.-M., Ma, W.-Y., and Lan, Y. UniGEM: A unified approach to generation and property prediction for molecules. In *Proceedings of the 13th International Conference on Representation Learning*, pp. 12824–12849, 2025.
- Fey, M. and Lenssen, J. E. Fast graph representation learning with pytorch geometric, 2019. URL <https://arxiv.org/abs/1903.02428>.
- Flam-Shepherd, D. and Aspuru-Guzik, A. Language models can generate molecules, materials, and protein binding sites directly in three dimensions as XYZ, CIF, and PDB files, 2023. URL <https://arxiv.org/abs/2305.05708>.

- Fu, C., Li, X., Olson, B., Ji, H., and Ji, S. Fragment and geometry aware tokenization of molecules for structure-based drug design using language models. In *Proceedings of the 13th International Conference on Learning Representations*. Curran Associates, Inc., 2025.
- Gebauer, N. W. A., Gastegger, M., and Schütt, K. T. Symmetry-adapted generation of 3D point sets for the targeted discovery of molecules. In *Proceedings of the 33rd Conference on Neural Information Processing Systems*, volume 32, pp. 7566–7578. Curran Associates, Inc., 2019.
- Gómez-Bombarelli, R., Wei, J. N., Duvenaud, D., Hernández-Lobato, J. M., Sánchez-Lengeling, B., Sheberla, D., Aguilera-Iparraguirre, J., Hirzel, T. D., Adams, R. P., and Aspuru-Guzik, A. Automatic chemical design using a data-driven continuous representation of molecules. *ACS Central Science*, 4:268–276, 2018. doi: 10.1021/acscentsci.7b00572.
- Ho, J., Jain, A., and Abbeel, P. Denoising diffusion probabilistic models. In *Proceedings of the 34th Conference on Neural Information Processing Systems*, volume 9, pp. 6840–6851. Curran Associates, Inc., 2020.
- Hoogeboom, E., Satorras, V. G., Vignac, C., and Welling, M. Equivariant diffusion for molecule generation in 3D. In *Proceedings of the 39th International Conference on Machine Learning*, volume 162, pp. 8867–8887. PMLR, 2022.
- Hua, C., Luan, S., Xu, M., Ying, R., Fu, J., Ermon, S., and Precup, D. MUDiff: Unified diffusion for complete molecule generation. In *Proceedings of the 2nd Learning on Graphs Conference*, volume 231. PMLR, 2023.
- Karpathy, A. NanoGPT, 2025. URL <https://github.com/karpathy/nanoGPT>. Accessed 2025-11-15.
- Kim, Y. and Kim, W. Y. Universal structure conversion method for organic molecules: From atomic connectivity to three-dimensional geometry. *Bull. Korean Chem. Soc.*, 36:1769–1777, 2015. doi: 10.1002/bkcs.10334.
- Kusner, M. J., Paige, B., and Hernández-Lobato, J. M. Grammar variational autoencoder. In *Proceedings of the 34th International Conference on Machine Learning*, volume 70, pp. 1945–1954. JMLR, 2017.
- Landrum, G. RDKit: Open-source cheminformatics, 2025. URL <https://www.rdkit.org>.
- Lee, J., Lee, Y., Kim, J., Kosiorek, A., Choi, S., and Teh, Y. W. Set transformer: A framework for attention-based permutation-invariant neural networks. In *Proceedings of the 36th International Conference on Machine Learning*, volume 97, pp. 3744–3753. PMLR, 2019.
- Li, H., Du, W., Li, Y., Guo, H., and Liu, S. InertialAR: Autoregressive 3D molecule generation with inertial frames, 2025a. URL <https://arxiv.org/abs/2510.27497>.
- Li, T., Tian, Y., Li, H., Deng, M., and He, K. Autoregressive image generation without vector quantization. In *Proceedings of the 27th Conference on Neural Information Processing Systems*, volume 37, pp. 56424–56445. Curran Associates, Inc., 2024. doi: 10.52202/079017-1797.
- Li, X., Wang, L., Luo, Y., Edwards, C., Gui, S., Lin, Y., Ji, H., and Ji, S. Geometry informed tokenization of molecules for language model generation. In *Proceedings of the 42nd International Conference on Machine Learning*, volume 267, pp. 36096–36128. PMLR, 2025b.
- Lipman, Y., Chen, R. T., Ben-Hamu, H., Nickel, M., and Le, M. Flow matching for generative modeling. In *Proceedings of the 11th International Conference on Learning Representations*. Curran Associates, Inc., 2023.
- Loshchilov, I. and Hutter, F. Decoupled weight decay regularization. In *Proceedings of the 7th International Conference on Learning Representations*. Curran Associates, Inc., 2019.
- Lu, S., Lin, H., Yao, L., Gao, Z., Ji, X., Liang, Y., E, W., Zhang, L., and Ke, G. Unified cross-scale 3D generation and understanding via autoregressive modeling, 2025. URL <https://arxiv.org/abs/2503.16278>.
- Luo, Y. and Ji, S. An autoregressive flow model for 3D molecular geometry generation from scratch. In *Proceedings of the 10th International Conference on Learning Representations*. Curran Associates, Inc., 2022.
- Peng, X., Luo, S., Guan, J., Xie, Q., Peng, J., and Ma, J. Pocket2Mol: Efficient molecular sampling based on 3D protein pockets. In *Proceedings of the 39th International Conference on Machine Learning*, volume 162, pp. 17644–17655. PMLR, 2022.
- Peng, X., Guan, J., Liu, Q., and Ma, J. MolDiff: Addressing the atom-bond inconsistency problem in 3D molecule diffusion generation. In *Proceedings of the 40th International Conference on Machine Learning*, volume 202, pp. 27611–27629. PMLR, 2023.
- Radford, A., Wu, J., Child, R., Luan, D., Amodei, D., Sutskever, I., et al. Language models are unsupervised multitask learners. *OpenAI blog*, 1(8), 2019.
- Ramakrishnan, R., Dral, P. O., Rupp, M., and Lilienfeld, O. A. V. Quantum chemistry structures and properties of 134 kilo molecules. *Scientific Data*, 1(140022), 2014. doi: 10.1038/sdata.2014.22.

- Satorras, V. G., Hoogeboom, E., Fuchs, F. B., Posner, I., and Welling, M. E(n) equivariant normalizing flows. In *Proceedings of the 35th Conference on Neural Information Processing Systems*, volume 34, pp. 4181–4192. Curran Associates, Inc., 2021.
- Schneuing, A., Harris, C., Du, Y., Didi, K., Jamasb, A., Igashov, I., Du, W., Gomes, C., Blundell, T. L., Lio, P., et al. Structure-based drug design with equivariant diffusion models. *Nat. Comput. Sci.*, 4:899–909, 2024. doi: 10.1038/s43588-024-00737-x.
- Simonovsky, M. and Komodakis, N. GraphVAE: Towards generation of small graphs using variational autoencoders. In *Proceedings of the 27th International Conference on Artificial Neural Networks*, pp. 412–422. Springer, 2018. doi: 10.1007/978-3-030-01418-6_41.
- Song, Y., Sohl-Dickstein, J., Kingma, D. P., Kumar, A., Ermon, S., and Poole, B. Score-based generative modeling through stochastic differential equations. In *Proceedings of the 9th International Conference on Learning Representations*. Curran Associates, Inc., 2021.
- Song, Y., Gong, J., Xu, M., Cao, Z., Lan, Y., Ermon, S., Zhou, H., and Ma, W.-Y. Equivariant flow matching with hybrid probability transport for 3D molecule generation. In *Proceedings of the 37th Conference on Neural Information Systems*, volume 36, pp. 549–568. Curran Associates, Inc., 2023.
- Song, Y., Gong, J., Zhou, H., Zheng, M., Liu, J., and Ma, W.-Y. Unified generative modeling of 3D molecules via bayesian flow networks. In *Proceedings of the 12th International Conference on Learning Representations*. Curran Associates, Inc., 2024.
- Su, J., Ahmed, M., Lu, Y., Pan, S., Bo, W., and Liu, Y. RoFormer: Enhanced transformer with rotary position embedding. *Neurocomputing*, 568(127063), 2024. doi: doi.org/10.1016/j.neucom.2023.127063.
- Tancik, M., Srinivasan, P. P., Mildenhall, B., Fridovich-Keil, S., Raghavan, N., Singhal, U., Ramamoorthi, R., Barron, J. T., and Ng, R. Fourier features let networks learn high frequency functions in low dimensional domains. In *Proceedings of the 34th International Conference on Neural Information Processing Systems*, pp. 7537–7547. Curran Associates, Inc., 2020.
- Tong, A., Fatras, K., Malkin, N., Huguet, G., Zhang, Y., Rector-Brooks, J., Wolf, G., and Bengio, Y. Improving and generalizing flow-based generative models with minibatch optimal transport, 2024. URL <https://arxiv.org/abs/2302.00482>.
- Vignac, C., Osman, N., Toni, L., and Frossard, P. MiDi: Mixed graph and 3D denoising diffusion for molecule generation. In *Proceedings of the Joint European Conference on Machine Learning and Knowledge Discovery in Databases*, pp. 560–576. Springer, 2023. doi: 10.1007/978-3-031-43415-0_33.
- Wang, Y., Lu, J., Jaitly, N., Susskind, J., and Bautista, M. A. SimpleFold: Folding proteins is simpler than you think, 2025a. URL <https://arxiv.org/abs/2509.18480>.
- Wang, Z., Shi, J., Heess, N., Gretton, A., and Titsias, M. Learning-order autoregressive models with application to molecular graph generation. In *Proceedings of the 42nd International Conference on Machine Learning*. PMLR, 2025b.
- Warr, W. A., Nicklaus, M. C., Nicolaou, C. A., and Rarey, M. Exploration of ultralarge compound collections for drug discovery. *J. Chem. Inf. Model.*, 62:2021–2034, 2022. doi: 10.1021/acs.jcim.2c00224.
- Xu, M., Powers, A. S., Dror, R. O., Ermon, S., and Leskovec, J. Geometric latent diffusion models for 3D molecule generation. In *Proceedings of the 40th International Conference on Machine Learning*, volume 202, pp. 38592–38610. PMLR, 2023.
- You, J., Ying, R., Ren, X., Hamilton, W., and Leskovec, J. GraphRNN: Generating realistic graphs with deep auto-regressive models. In *Proceedings of the 35th International conference on machine learning*, volume 80, pp. 5708–5717. PMLR, 2018.
- Zaheer, M., Kottur, S., Ravanbakhsh, S., Poczos, B., Salakhutdinov, R. R., and Smola, A. J. Deep sets. In *Proceedings of the 31st Conference on Neural Information Processing Systems*, volume 30. Curran Associates, Inc., 2017.
- Zhang, L., Ashouritaklimi, K., Teh, Y. W., and Cornish, R. SymDiff: Equivariant diffusion via stochastic symmetrisation, 2025. URL <https://arxiv.org/abs/2410.06262>.

A. Appendix

A.1. Extended Related Works

Diffusion Models for 3D Molecular Generation Diffusion models represent the current state of the art in 3D molecular generation. These models (Ho et al., 2020; Song et al., 2021) operate by progressively corrupting the training data with random noise through a forward diffusion process, and training a neural network to reverse this corruption via step-by-step denoising. During inference, new samples are generated by iteratively applying the learned reverse diffusion process to random noise. Prominent diffusion-based molecular generation models include EDM (Hoogeboom et al., 2022), MiDi (Vignac et al., 2023), GeoLDM (Xu et al., 2023), GeoBFN (Song et al., 2024), and SymDiff (Zhang et al., 2025). They have been successfully employed in multiple applications, but they do have notable limitations. First, they require the number of atoms in a generated molecule to be pre-specified, which can be addressed using dummy atom tokens. However, this imposes an upper bound on molecule size. Second, diffusion models use computationally expensive message-passing operations at each step of the stochastic differential equation (SDE) integration to capture atom interdependencies. This results in high computational costs during inference.

Flow Matching Flow matching (Lipman et al., 2023; Albergo & Vanden-Eijnden, 2023) offers a conceptually simple alternative to diffusion models and often achieves faster inference due to the need for fewer integration steps during the inference process. It is a simulation-free training framework for generative modeling, where a time-dependent velocity field ψ_t is learned to couple a tractable source distribution p_0 with a target distribution p_1 . Typically, p_0 is chosen as a standard normal distribution, $p_0 = \mathcal{N}(\mathbf{0}, \mathbf{I})$, and the transport is defined over a time interval $t \in [0, 1]$. The transformation of p_0 into intermediate distributions p_t is achieved via the push-forward operation $\#$, resulting in a trajectory of probability distributions $p_t(\mathbf{x}_t)$ at time t . The flow ψ_t is modeled using a parameterized function $\mathbf{v}_\theta(\mathbf{x}_t, t)$, which is trained to approximate the velocity field. Sampling from the target distribution p_1 is performed by drawing samples $\mathbf{x}_0 \sim p_0$ and integrating the ordinary differential equation (ODE) $d\mathbf{x}_t = \mathbf{v}_\theta(\mathbf{x}_t, t)$.

Lipman et al. (2023) introduced simulation-free training by constructing conditional probability paths. A widely used choice for these paths is the linear interpolant (Albergo & Vanden-Eijnden, 2023), defined as $\mathbf{x}_t = t\mathbf{x}_1 + (1-t)\mathbf{x}_0$, with the conditional target velocity $\mathbf{v}_t = \mathbf{x}_1 - \mathbf{x}_0$. The training objective, known as conditional flow matching (CFM), minimizes the l_2 regression loss: $\mathcal{L}_{\text{CFM}} = \mathbb{E}[\|\mathbf{v}_\theta(\mathbf{x}_t, t) - \mathbf{v}_t\|]$. Flow-matching-based molecular generation models include EquiFM (Song et al., 2023) and FlowMol3 (Dunn & Koes, 2025). Independent coupling of p_0 and p_1 can result in high transport costs and intersecting conditional paths. These issues can be alleviated by employing optimal transport couplings between the source and target distributions, thereby improving convergence and enhancing flow performance (Tong et al., 2024). In molecular generation, this has been approached, *e. g.*, through rigid alignment of noisy and true coordinates, combined with solving the assignment problem to minimize transport costs (Dunn & Koes, 2025).

A.2. Implementation Details

System and Software specification Training was performed on a Rocky Linux 9.4 system with an NVIDIA RTX Pro 6000 Blackwell Graphics Processing Unit with 96 GB GDDR7 VRAM and an AMD EPYC 9555 64-Core Processor. We use CUDA 13.0 for GPU acceleration. Our model is implemented in Python (v3.11.13) with PyTorch (v2.8.0), PyTorch Geometric (v2.7.0) (Fey & Lenssen, 2019), and Pytorch Lightning (v2.5.5) (Falcon & the PyTorch Lightning team, 2025). Model training was monitored with Tensorboard (v2.20.0). For chemical data processing we employed RDKit (v2025.9.1) (Landrum, 2025). For visualization, we used Py3Dmol (v2.5.3), plotting was performed with matplotlib (v3.10.7).

Model The basis of our implementation is the NanoGPT implementation of Karpathy (2025), which provides a concise implementation of the GPT-2 (Radford et al., 2019) model. We do not use bias in the layers of the transformer module. For positional encoding of the Cartesian coordinates, we employ Fourier features (Tancik et al., 2020) as implemented in (Wang et al., 2025a). We experimented with qk-normalization and rotary position embeddings (Su et al., 2024), but did not find improved results. We found additive pooling the most promising pooling strategy, but also tried mean and attention pooling. We also tried local attention, defined by a radius graph, instead of full attention over all atom nodes, which led to performance degradation. Inclusion of charged states into the atom type vocabulary did not lead to model improvement. Since our model architecture is not $SE(3)$ -equivariant, we augment data samples by random rotation, which stabilizes the training. We experimented with random translations as well, however, we did not find an increase in model performance. The flow matching head is the same adaptive layer-norm MLP as used in Li et al. (2024), which was also used in the QUETZAL model (Cheng et al., 2025) for implementation of the diffusion head.

Source-target split The splitting procedure in Algorithm 1 is governed by the hyperparameters β and γ (see Section 3). Figure 4 reports the absolute and relative (*w.r.t.* the original graphs) source and target set sizes for a batch of 25,000 training graphs. Across all runs, we used $\beta = 1.5$ and $\gamma = 0.55$. These settings produced an approximately uniform source set distribution with a slight bias toward smaller sets. The resulting target sets contain on average $\sim 18\%$ of the nodes of the original graphs. We also evaluated source-set distributions emphasizing mid-sized to larger sets, but near-uniform sampling performed best.

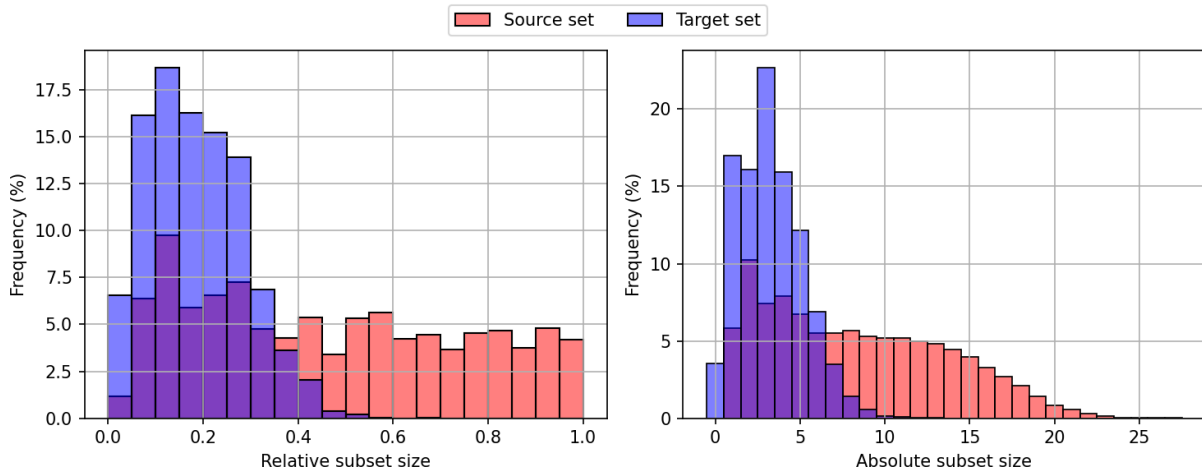


Figure 4. Relative and absolute size distribution of the source and target set *w.r.t.* the original graphs. Sampling was performed with $\beta = 1.5$ and $\gamma = 0.55$.

Time step sampling For training the flow matching head, we sample random time steps analog to the SimpleFold model (Wang et al., 2025a) from the following log-normal distribution:

$$p(t) = 0.02\mathcal{U}(0, 1) + 0.98\text{LN}(0.8, 1.7) \quad (6)$$

with

$$\text{LN}(t; m, s) = \frac{1}{t(1-t)s\sqrt{2\pi}} \exp\left(-\frac{(\text{logit}(t) - m)^2}{2s^2}\right) \quad (7)$$

where we set $m = 0.8$ and $s = 1.7$. With these settings, time steps are sampled more densely around $t = 1$. We found that this sampling schema slightly improved training above time step sampling from a uniform distribution. For each conditional path, we sampled 16 random time steps. While we found resampling to be beneficial, using more than 16 time steps per path did not have an impact on model convergence. We found Euler integration with equidistant time steps to be sufficient for integration of the flow ODE. We also tried a Runge-Kutta-4 and an adaptive time step Dormand-Prince integrator, but could not find improved performance. Using endpoint parametrization for construction of the conditional paths, like done in Dunn & Koes (2025), led to performance degradation.

Hyperparameters The hyperparameters of our best performing model are summarized in Table 2. The loss function was minimized with the AdamW (Loshchilov & Hutter, 2019) optimizer using a learning rate of $1 \cdot 10^{-4}$, parameters $\beta_1 = 0.9$ and $\beta_2 = 0.95$, and a weight decay of $1 \cdot 10^{-6}$. We further used gradient clipping to 1.0 of the gradient norm. We experimented with different learning rates and found that increasing the learning rate led to exploding gradients. We implemented a cosine annealing learning rate schedule with 50 linear warm-up epochs and set the minimum learning rate to 10% of the initial learning rate after 10,000 epochs. Model training took 96 hours, given the above hardware specifications.

A.3. Additional Results & Comparisons

Comparison to diffusion models In Table 3, we compare NEAT to six diffusion models (EDM (Hoogeboom et al., 2022), MiDi (Vignac et al., 2023), GeoLDM (Xu et al., 2023), GeoBFN (Song et al., 2024), SymDiff (Zhang et al., 2025), UniGEM (Feng et al., 2025)) in addition to the autoregressive baselines.

Table 2. Hyperparameters of the best performing model on the QM9 dataset

Parameter	Value
batch size	2048
β	1.5
bias	true
dropout	0.1
epochs	10,000
γ	0.55
flow matching head hidden dimension	1,536
flow matching head layers	6
flow matching noise standard deviation σ	1.4
learning rate	10^{-4}
learning rate decay number of epochs	10,000
learning rate minimum	10%
learning rate warm-up number of epochs	50
time step resampling	16
time step sampling	logit normal
transformer heads	16
transformer hidden dimension	1,024
transformer layers	16
vocabulary size	6
weight decay	10^{-6}

 Table 3. Performance comparison of NEAT with diffusion (middle block) and autoregressive (lower block) models trained on the QM9 dataset. All values are given in percent. The **best** and second-best performing models are highlighted. Models evaluated using our pipeline are marked with a star (*). Metrics are reported as the mean and 95% confidence interval over three runs, each generating 10,000 molecular designs. Results in the top block are computed on the QM9 test set of 13,083 molecules.

metrics	atom stab.	mol. stab.	lookup valid	lookup unique	xyz2mol valid	xyz2mol unique
QM9	99.4	95.3	97.7	97.7	100	100
EDM	98.7	82.0	91.9	90.7	86.7	86.0
MiDi	97.9	84.0	97.9	97.0	n.a.	n.a.
GeoLDM	<u>98.9</u>	89.4	93.8	92.7	91.3	90.3
GeoBFN	99.3	93.3	96.9	92.4	n.a.	n.a.
SymDiff	<u>98.9</u>	89.7	96.4	94.1	92.8	91.4
UniGEM	<u>98.9</u>	<u>93.2</u>	95.0	<u>93.2</u>	n.a.	n.a.
G-SchNet	95.7	68.1	85.5	80.3	75.0	72.5
Symphony	90.8	43.9	68.1	66.5	83.5	81.8
Geo2Seq	<u>98.9</u>	<u>93.2</u>	<u>97.1</u>	81.7	n.a.	n.a.
QUETZAL*	98.3	87.5	94.6	90.1	99.3	<u>94.4</u>
	± 0.1	± 0.1	± 0.1	± 0.2	± 0.1	± 0.1
NEAT*	98.2	84.7	93.4	88.6	<u>98.5</u>	94.8
	± 0.1	± 0.4	± 0.3	± 0.4	± 0.1	± 0.1

Generated Molecules Figure 5 and 6 show 3D and 2D plots of 35 randomly selected molecules generated by NEAT after being trained on the QM9 dataset.

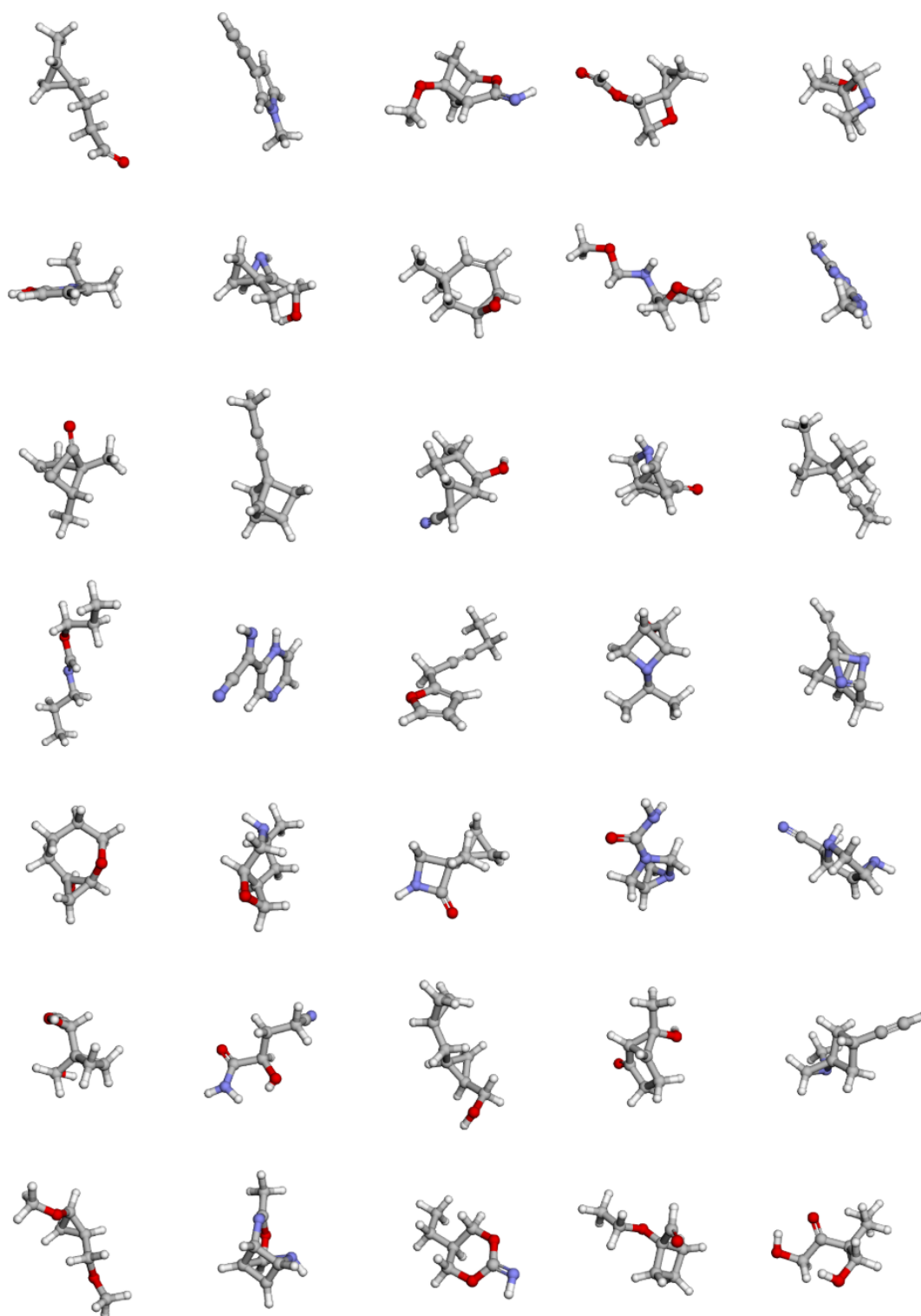


Figure 5. Randomly selected molecules generated by NEAT after being trained on the QM9 dataset (white: hydrogen, gray: carbon, blue: nitrogen, red: oxygen, green: fluorine). 2D plots of the same molecules are shown in the next figure.

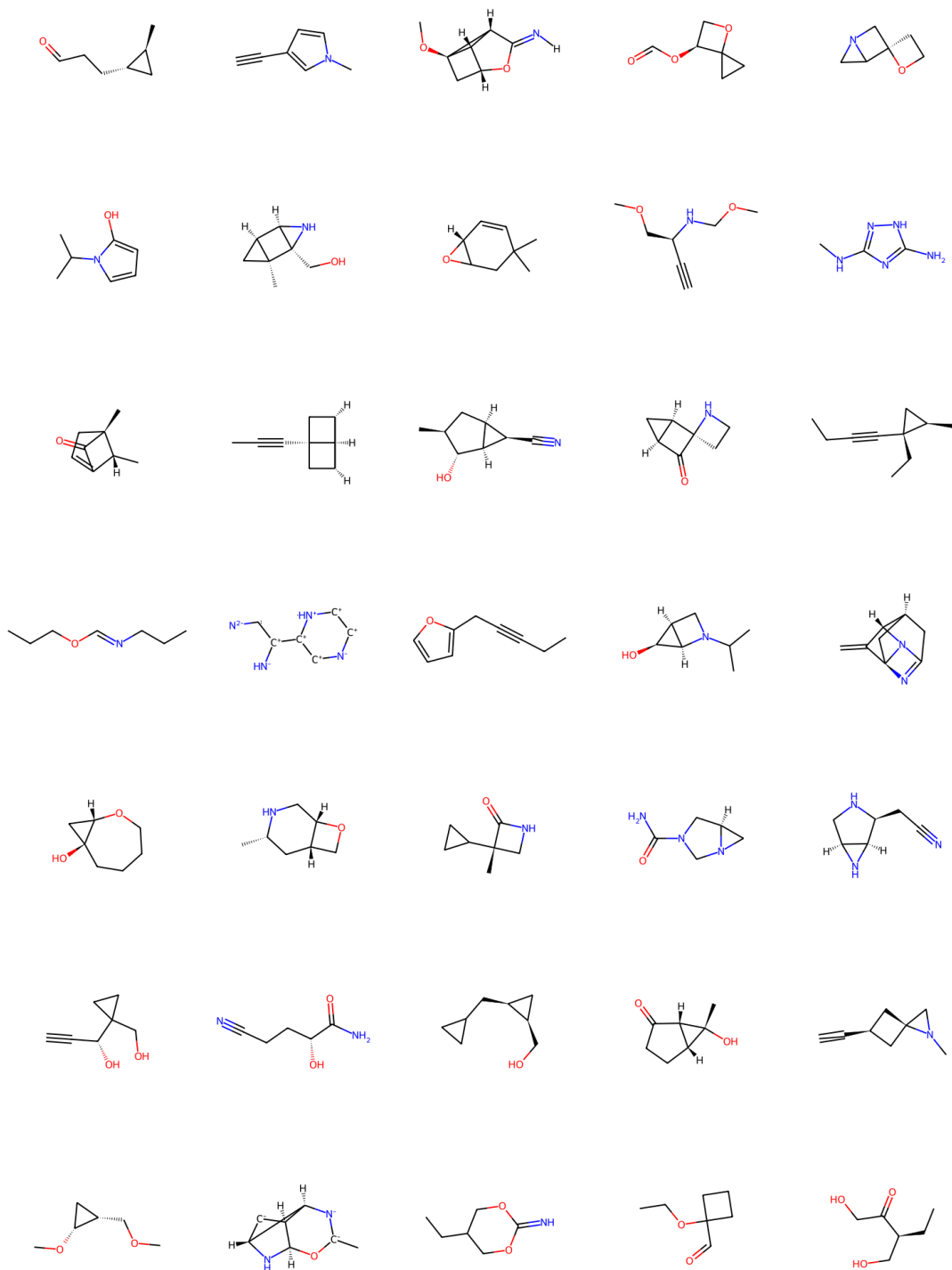


Figure 6. Randomly selected molecules generated by NEAT after being trained on the QM9 dataset (white: hydrogen, gray: carbon, blue: nitrogen, red: oxygen, green: fluorine). Implicit hydrogen atoms have been removed for the sake of clarity. 3D plots of the same molecules are shown in the previous figure.